X-ray diffraction of molybdenum under shock compression to 450 GPa

Jue Wang, Federica Coppari, Raymond F. Smith, Jon H. Eggert, Amy E. Lazicki, Dayne E. Fratanduono, J. Ryan Rygg, Thomas R. Boehly, Gilbert W. Collins, and Thomas S. Duffy

Phys. Rev. B **92**, 174114 — Published 20 November 2015

DOI: 10.1103/PhysRevB.92.174114

X-Ray Diffraction of Molybdenum Under Shock Compression to 450 GPa

Jue Wang[1], Federica Coppari[2], Raymond F. Smith[2], Jon H. Eggert[2], Amy E. Lazicki[2], Dayne E. Fratanduono[2], J. Ryan Rygg[2], Thomas R. Boehly[3], Gilbert W. Collins[2], and Thomas S. Duffy[1]
[1]*Department of Geosciences, Princeton University, Princeton, NJ, 08544*
[2]*Lawrence Livermore National Laboratory, P.O. Box 808, Livermore, California 94550*
[3]*Laboratory for Laser Energetics, University of Rochester, 250 East River Road, Rochester, New York 14623-1299*

Molybdenum (Mo) is a body-centered-cubic (BCC) transition metal that has widespread technological applications. While the BCC transition elements are used as test cases for understanding the behavior of metals under extreme conditions, the melting curves and phase transitions of these elements have been the subject of stark disagreements in recent years. Here we use X-ray diffraction to examine the phase stability and melting behavior of Mo under shock loading to 450 GPa. The BCC phase of Mo remains stable along the Hugoniot until 380 GPa. Our results do not support previous claims of a shallow melting curve for molybdenum.
PACS numbers: 61.05.cp, 64.70.D-, 62.50.ef

I. Introduction

Molybdenum is a refractory, high-strength metal that is technologically important. In recent year its phase stability, equation of state, and melting behavior have been the subject of intensive investigation[1–9]. The equation of state of molybdenum has been well studied using static compression techniques[10–14] with recent work[15] demonstrating that Mo remains in the body centered cubic (BCC) phase until at least 410 GPa at room temperature. Molybdenum is utilized as an equation-of-state standard in shock compression experiments[16–19] and for pressure calibration in the diamond anvil cell[13,20,21].

The phase diagram of molybdenum at high pressures and temperatures is the subject of considerable on-going controversy. Early sound velocity measurements[2] under shock loading identified two discontinuities -- at 210 GPa (~4100 K) and at 390 GPa (~10,000 K) that were interpreted as solid-solid and solid-liquid transitions, respectively. In contrast, static diamond anvil cell (DAC) experiments[1,3] on Mo up to 119 GPa reported a very shallow melting slope and comparison with shock data was used to infer that the reported 210-GPa discontinuity was associated with melting while the higher pressure discontinuity could be connected to a structural change in the liquid[22]. The discrepancy between the static and shock data is considerable with differences in melting temperature of thousands of Kelvin at megabar pressures.

Theoretical methods using density functional theory (DFT) and molecular dynamics have also been used to calculate the melting curve of Mo at high pressures. These studies consistently find a steep melting slope that is in much better agreement with the shock wave data than the diamond anvil cell measurements[4,8,23–25]. First-principles calculations on BCC metals such as Mo are expected to be reliable based on their ability to reproduce experimental results for a wide range of properties (equation of state, thermoelastic properties, etc.) over a broad pressure range[8]. However, it has been argued that such methods may not be accurate for melting of BCC metals if there are substantial changes in the electronic structure upon melting[26].

Theoretical studies have also addressed the question of solid-solid phase transitions in molybdenum at high P-T conditions. Initial studies using DFT predicted a transition to a face centered cubic (FCC) or hexagonal close packed (HCP) phase at pressure-temperature conditions that could explain the 210-GPa discontinuity in shock wave data[4–7]. However, a more recent theoretical calculation that fully included the effect of anharmonicity for the first time found instead that the BCC phase remained stable up to melting, and no explanation for the 210-GPa discontinuity could be provided[8]. Recently, the sound velocities of shocked molybdenum were re-measured[9] and, in agreement with the theoretical calculation[8], it was found that there is no statistically significant evidence for a 210-GPa discontinuity, thereby suggesting that Mo remains in the BCC phase until shock melting near 390 GPa. However, other recent studies have already raised questions about this conclusion[27,28].

Similar controversies surround the melting curve and phase stabilities of other transition metals[1] including Ta[29–32] and Fe[33–36], so a better understanding of Mo has broader implications for high-pressure science and geophysics. Previous shock wave studies of molybdenum provided only constraints on the equation of state[16] or sound velocities[2,9,37] and could not directly determine the stability of different phases. Laser-driven dynamic compression experiments have emerged in recent years as a novel technique for probing the ultra-high pressure behavior of materials[38–40]. In laser-shock experiments, the application of pulsed high-powered laser energy ablates the surface of a sample creating a hot, expanding plasma which exerts pressure on the surrounding material resulting in the propagation of a strong shock wave through the sample. The development of nanosecond X-ray diffraction diagnostics provides a new means to probe the lattice compression and structural state of materials under these extreme conditions[41–44]. Here we use powder X-ray diffraction on laser-shock-compressed molybdenum to directly probe the phases on the Hugoniot up to 450 GPa.

II. Experimental Techniques

Our experiments were carried out at the Omega Laser Facility[45], which is a 351-nm, 60-beam Nd:glass laser with up to 500 J of energy per beam. Targets consisted of an 11-μm-thick Mo foil (GoodFellow Corp., 99.9% purity) attached with thin (~1 μm) epoxy layers between a 25-μm-thick polyimide (CH) layer and a 120-μm-thick LiF window (Fig. 1). The starting Mo foils were characterized by X-ray diffraction which revealed a texture with (200) and (211) planes normal to the foil. A 3.7-ns long laser pulse with energy ranging from 50-124 J was focused to a diameter of 800 μm on the surface of the polyimide layer. Ablation of this surface resulted in a ~1-3 ns duration shock wave propagating through the polyimide and into the molybdenum sample. The response of the sample was monitored using velocity interferometry and X-ray diffraction.

Velocity interferometry (VISAR, Velocity Interferometer System for Any Reflector[46]) was used to measure the particle velocity history after shock arrival at the Mo/LiF interface (Fig. 2). The measured interface velocity was used together with the known shock velocity (U_S) – particle velocity (u_p) relationships for Mo and LiF to determine the pressure in the shocked Mo using the impedance matching method[47]. The equation of state data for these two materials were obtained by fitting experimental gas gun data for Mo[16–18,48–50] and LiF[50–53] to a linear relationship:

$$U_S = c + su_p, \quad (1)$$

where c and s are constants (Table I). Release adiabats were approximated by reflecting the Hugoniot in the P-u_p plane. The uncertainty in interface velocity was determined from the uncertainty in the measured fringe shift and the velocity uncertainty over the field of the view. The error in pressure was determined from propagation of uncertainties in the measured shock and interface velocities and the equation of state parameters.

Powder X-ray diffraction was used to probe the structure and volume compression of shocked molybdenum[43,44,54]. The sample assembly was attached to a 300-μm-diameter Ta pinhole and mounted on the front of an X-ray enclosure (Fig. 1). A nanosecond X-ray source was generated by focusing sixteen beams of the Omega laser with energy of 500 J/beam in a ~1 ns long pulse to a ~310-420-μm diameter spot onto a 2-mm square, 13-μm-thick copper foil. The foil was mounted 30 mm from the target at an angle of 45°. Irradiation of the foil generated a source of quasi-monochromatic He-α X-rays at 8.38 keV with bandwidth of ~2%[43]. Satellite peaks in the emitted x-ray spectrum are suppressed using filtering[43]. The X-rays passed through the Mo sample and were collimated by the Ta pinhole. The X-ray emission was timed such that the sample is probed while the shock front is propagating through the Mo layer but has not yet reached the Mo/LiF interface. X-ray diffraction lines generated from the target package were recorded on image plates (IPs) lining the walls of the enclosure (Fig. l). Typical diffraction peak widths were ~1° and diffraction angles could be resolved to ~0.1°.[43] Computer simulations were carried out using the hydrocode HYADES[56] in order to determine the laser pulse shapes and power levels required to achieve the desired pressures in the Mo sample. The simulations were also used to determine the time delay required between the laser pulse that compresses the sample and the pulse that generates the X-ray source. The initial estimates of the laser powers and time delays from the simulations were modified as necessary over the course of the experiments to optimize the obtained results.

III. Results

A series of experiments was performed in which molybdenum was shock compressed over the range from 250-450 GPa. Figures 3 and 4 show representative X-ray diffraction results for shock-compressed Mo at different pressures. Figure 3 shows raw (no background subtraction) X-ray images from a single image plate (panel labeled "L" in Fig. 1). For each image, the observed diffraction lines can be assigned to one of the following: 1. Mo at ambient pressure (from the uncompressed region of the sample in front of the on-coming shock wave); 2. shock-compressed Mo; 3. ambient-pressure Ta (from the pinhole). The diffraction geometry was calibrated using the ambient-pressure diffraction lines from uncompressed Mo and Ta[43]. In Figure 4 (panels a, c, e, and g), the full diffraction images at selected pressures have been projected into 2θ-ϕ space[43], where 2θ is the diffraction angle and ϕ is the azimuthal angle around the incident X-ray direction. This figure (panels b, d, f, and h) also shows one-dimensional diffraction patterns from selected regions of the images.

At 250 GPa, a strong diffraction line was observed at *d*-spacing of 1.948(9) Å (orange arrows in Fig. 3a and 4a,b) that can be assigned to the highest intensity (110) peak of Mo in the BCC structure. The corresponding ambient-pressure (110) peak is also observed in these shots (red arrow in Fig. 3). This indicates that the BCC phase remains stable above the pressure of the previously reported 210-GPa sound velocity discontinuity and further implies that this discontinuity is not related to melting as suggested in previous DAC experiments[1,3]. At higher pressures, the (110) peak from compressed Mo remains observable while shifting to lower *d*-spacings (higher 2θ) with compression (Fig. 3b-d, 4c,d).

The densities of crystalline Mo determined from the unit cell volume obtained from the measured (110) *d*-spacings of the BCC structure up to 380 GPa are shown in Fig. 5 and Table II. Densities calculated independently from impedance matching using the known equations of state for Mo and LiF are within 1% of those obtained directly from x-ray diffraction. Also shown in Fig. 5 are previous gas-gun Hugoniot data[16–18,48,50] (grey diamonds) and 293-K static compression data from diamond anvil cell experiments[13,21] (red triangles). The densities obtained from our X-ray diffraction on laser-shocked Mo (black symbols) are consistent with the previous gas-gun Hugoniot data within uncertainty. This supports the assignment of the observed diffraction line to the (110) peak of BCC Mo.

Previous theoretical studies predicted that a phase transition to the FCC or HCP structures may occur at high pressures and temperatures along the Hugoniot in Mo[4–7]. Other candidate high-pressure phases include the double hexagonal close packed structure (dHCP) and the hexagonal omega (ω) phase[5,57]. Our observed high-pressure Mo diffraction peak has been assigned to the (110) peak of the BCC structure. The validity of this peak assignment is supported by the agreement between the density from x-ray diffraction with that from the measured particle velocity and the known equation of state of Mo. However, we must also consider whether this single diffraction peak could instead arise from one of the alternative structures for Mo at high pressure. Using the measured *d*-spacing, we tested other phases by calculating the density that would result from assignment of the observed peak to lines from those other structures. To do this, we identified the diffraction line from each candidate structure that would provide the closest match to the density obtained from the equation of state measurement. The corresponding lines are (111) for FCC, (002) for HCP, (004) for dHCP and (101) or (110) for ω. The resulting density from assignment to the FCC (111) and HCP (002) lines is about 9% greater than obtained by assigning the line to the BCC (110) reflection. These densities for FCC and HCP structures are inconsistent with the stress-density response of Mo measured in gas-gun Hugoniot experiments and therefore these structures can be rejected (Fig. 5). All other diffraction lines of these phases also give unreasonable densities and/or *c/a* ratios when fit to our observation.

If the diffraction peak is assigned to the dHCP or ω phase, the densities would be 1.4% greater than that of the BCC phase and are marginally consistent with the Hugoniot data (Fig. 5). The ω phase is a hexagonal structure (*P6/mmm*) arising from a distortion of the BCC phase in which the BCC (110) peak is replaced by a doublet of near equal intensities whose separation depends on the *c/a* ratio. Since we observe no evidence for a doublet or peak splitting in our diffraction data, an ω phase distortion along the Mo Hugoniot is not consistent with our data. In addition, theoretical calculations suggest the

ω phase is not stable in Mo at high pressures[57]. For dHCP, the only diffraction peak which gives marginally plausible densities is the (004) peak which for an untextured solid would be expected to have significantly lower peak intensity than other neighboring peaks (only 30% intensity of the (102) peak). This is not consistent with our observations of only a single detectable diffraction peak in Mo. On the other hand, the (110) peak of the BCC structure is expected to have intensities that are 3-6 times greater than the next closest (200) and (211) reflections, and is thus consistent with our observation of only a single diffraction line. Hence, our measured diffraction data cannot be explained by any other structure than the BCC phase at high pressures.

Starting from 390 GPa, the (110) diffraction line from Mo becomes broad and weak (Figs. 3e,f; 4e,g). The observed peak has a width (full width at half maximum, FWHM, of 4.2-4.4°) that is considerably larger than the compressed Mo peaks at lower pressures (FWHM =1.6-1.9°) (Fig. 6a). The broad feature also exhibits nearly constant intensity along its azimuth, in contrast with the textured signal observed at lower pressure (Fig. 6b,c). These observations are consistent with loss of crystallinity indicating that melting initiates along the Hugoniot near 390 GPa. Along the Hugoniot, the melting transition occurs over a finite pressure interval until sufficient energy is supplied to completely melt the solid[58], and thus our observed signal likely represents a mixture of solid and liquid material.

IV. Discussion

Our X-ray diffraction measurements provide a direct determination of shock melting in Mo at 380-390 GPa, supporting the previous interpretation of Hugoniot sound velocity measurements[2,9]. The expected shock temperatures at this pressure are also consistent with the expected melting temperature of Mo from *ab initio* molecular dynamics at these pressures. Figure 7 summarizes the phase diagram of Mo including our new Hugoniot results. The temperature achieved in shock-compressed molybdenum were calculated by Ref. 58 using the thermodynamic relationship:

$$dT = -\frac{\gamma T}{V} dV + \frac{(V_0 - V)dP + PdV}{2C_V}, \qquad (2)$$

where γ is the Grüneisen parameter and C_V is the heat capacity. Also shown in the figure are previous DAC melting data[1,3] and locations of reported shock sound speed discontinuities[2] (green crosses). The Hugoniot temperatures, T_H, shown in Figure 7 from Ref. 58 are generally consistent with calculated Hugoniot temperatures from other studies[2,16,59] which yield T_H = 3700-4100 K at 210 GPa and T_H=8040-10,000 K at 390 GPa. A measurement of the shock temperature of Mo by pyrometry[59] reported a value of 7853±813 K at 374 GPa which is consistent with calculated values. Theoretical studies[4,24] using *ab initio* molecular dynamics yield values of 8300-9300 K for the melting temperature at 390 GPa, also in reasonable agreement with the Hugoniot calculations and measurements. The rapid heating during shock compression can result in superheating of the solid above the melting temperature[60]. Applying the results of a systematic study of superheating behavior in elements and simple compounds[60], it is estimated that superheating may reduce the calculated shock temperatures at 390 GPa by ~30% to 7700±1500 K which is in good agreement with the theoretical melting curves[4,24] but well above extrapolated DAC melting results (Fig. 7).

The persistence of the (110) diffraction peak of BCC molybdenum to high pressures also raises questions regarding the origin of the 210-GPa sound velocity discontinuity observed by Ref. 2. Recently, a gas gun study[9] has repeated the measurement of sound velocities on shock-loaded Mo to pressures above 400 GPa (Fig. 8). In this work, they confirmed the previous findings that melting occurs along the Hugoniot near 390 GPa, but found no evidence for a compressional sound velocity discontinuity near 210 GPa. This indicates that a phase transition at this pressure is unnecessary. However, Errandonea et al[27] have reinterpreted this same dataset to suggest that partial melting of Mo begins near 240 GPa. In addition, recent *ab initio* calculations of the compressional sound velocity in BCC Mo along the Hugoniot show discrepancies with the measurements of Ref. 2 that were interpreted as evidence for a solid-solid phase transition[28] .

Measured and calculated sound velocities[2,9,28,37] for Mo are summarized in Figure 8. Compressional sound velocities, V_P, are obtained gas gun measurements using the optical analyzer technique[2,9,37]. Bulk sound velocities, V_B, taken from Ref. 2, are calculated from the local slope of the Hugoniot curve together with the assumption that $\rho\gamma$ = constant, where ρ is the density and γ is the Grüneisen parameter. The shear wave velocity along the Hugoniot is calculated from the relationship: $V_S^2 = 3/4(V_P^2 - V_B^2)$. Also shown are the recent *ab initio* calculations of Ref. 28. Taken together, the measured V_P values show clear evidence only for a single sound velocity discontinuity near 380-400 GPa and a discontinuity near 210 GPa is not observed.

The *ab initio* bulk sound velocities[28] for molybdenum are in good agreement with those calculated from the Hugoniot slope[2] but the compressional velocity values diverge increasingly from the Hugoniot measurements at high pressures (Fig. 8). Lukinov et al.[28] suggest this may be evidence for a possible solid-solid phase transition above 200 GPa. However, phase transitions typically produce a discontinuity in the sound velocity which is not observed here. Alternatively, the discrepancy may be related to limitations in accuracy of the theoretical calculations. A further possibility is that the discrepancy can be due to deviations of the measured sound velocities from that of an isotropic aggregate. From the reported elastic constants[28], C_{ij}, we calculated the Zener anisotropy factor: $A = 2C_{44}/(C_{11}-C_{12})$. The elastic anisotropy of Mo increases along the Hugoniot from a modest value (A=1.40) at 136 GPa to a value of 4.3 at 330 GPa, indicating a substantial increase in elastic anisotropy with compression. The high degree of elastic anisotropy together with the presence of texturing in the compressed material may cause the measured velocities to deviate from those of an isotropic average reported by Ref. 28.

Our x-ray diffraction measurements provide direct evidence for the stability of BCC Mo to pressures well above the 210-GPa "discontinuity". As discussed above, this is supported by recent re-measurements of Hugoniot sound velocities[9] which show no direct evidence for such a discontinuity. Additional evidence for the stability of BCC Mo above 210 GPa is provided by the recent theoretical study[8] in which anharmonic effects on Mo lattice vibrations are taken into account. In contrast to earlier work[4,5,7], this study found that the BCC phase remains stable at high P-T conditions up until melting, in agreement with our experimental results. Thus our finding that Mo remains in the BCC structure to 380 GPa is consistent with both the most advanced theoretical calculations and the latest sound velocity measurements.

The shear velocities calculated from the Nguyen et al. data[9] exhibit softening beginning from about 240 GPa (Fig. 8) and Errandonea et al[27]suggest this may be related to the beginning of partial melting along the Hugoniot, potentially reconciling the shock data with the low melting temperatures obtained in diamond anvil cell experiments. However, softening of the shear velocity is not conclusive evidence for partial melting as the rapid increase in shock temperature at these pressures may produce thermal softening in the solid state. Notably, the shear velocities obtained from the *ab initio* calculations[28] on solid Mo along the Hugoniot also exhibit softening with increasing pressure in this range (Fig. 8). Softening of the shear modulus along the Hugoniot has been observed experimentally in copper and other metals in the solid state[61,62]. Furthermore, the theoretically calculated melting temperatures near 210 GPa (T_m=6600-7250 K)[4,24] lie well above the expected Hugoniot temperatures (3700-4100 K), so partial melting is not expected at these conditions. Melting temperature measurements in DAC experiments may suffer uncertainties due to temperature gradients, systematic temperature measurement error, and ambiguous melt criteria and these factors could lead to an underestimate of melting temperatures[63].

V. Conclusions

In summary, we show that X-ray diffraction combined with laser-driven shock compression can be used to provide direct constraints on lattice structure and melting to very high pressures. Shock-compressed molybdenum shows no evidence of a solid-solid phase transition along the Hugoniot; the BCC structure remains stable until shock melting begins at ~390 GPa. Previous suggestions of a low melting temperature for Mo are not supported by our data. Our results are in good agreement with recent theoretical calculations accounting for anharmonicity[8] and recent re-measurement of sound speeds along the Hugoniot[9,37], which together provide a consistent description of the high-pressure behavior of this fundamental transition metal.

Acknowledgements

We thank the operations staff at the Omega Laser and the Target Engineering Team at Lawrence Livermore National Laboratory (LLNL) for their assistance in these experiments. Richard Kraus (LLNL) and an anonymous reviewer provided helpful comments on the manuscript. The research was supported by NNSA/DOE through the National Laser Users' Facility Program under contracts DE-NA0000856 and DE-FG52-09NA29037 and the Laboratory Directed Research and Development program at LLNL (project number 12-SI-007). This work was performed under the auspices of the US Department of Energy by Lawrence Livermore National Laboratory under contract number DE-AC52-07NA27344.

References

[1] D. Errandonea, B. Schwager, R. Ditz, C. Gessmann, R. Boehler, and M. Ross, Phys. Rev. B **63**, 132104 (2001).
[2] R.S. Hixson, D.A. Boness, J.W. Shaner, and J.A. Moriarty, Phys. Rev. Lett. **62**, 637 (1989).

[3] D. Santamaría-Pérez, M. Ross, D. Errandonea, G.D. Mukherjee, M. Mezouar, and R. Boehler, J. Chem. Phys. **130**, 124509 (2009).
[4] A. Belonoshko, L. Burakovsky, S. Chen, B. Johansson, A. Mikhaylushkin, D. Preston, S. Simak, and D. Swift, Phys. Rev. Lett. **100**, 135701 (2008).
[5] A.S. Mikhaylushkin, S.I. Simak, L. Burakovsky, S.P. Chen, B. Johansson, D.L. Preston, D.C. Swift, and A.B. Belonoshko, Phys. Rev. Lett. **101**, 049602 (2008).
[6] C. Cazorla, D. Alfè, and M. Gillan, Phys. Rev. Lett. **101**, 049601 (2008).
[7] Z.-Y. Zeng, C.-E. Hu, L.-C. Cai, X.-R. Chen, and F.-Q. Jing, J. Phys. Chem. B **114**, 298 (2010).
[8] C. Cazorla, D. Alfè, and M.J. Gillan, Phys. Rev. B **85**, 064113 (2012).
[9] J.H. Nguyen, M.C. Akin, R. Chau, D.E. Fratanduono, W.P. Ambrose, O.V. Fat'yanov, P.D. Asimow, and N.C. Holmes, Phys. Rev. B **89**, 174109 (2014).
[10] B. Godwal and R. Jeanloz, Phys. Rev. B **41**, 7440 (1990).
[11] L. Ming and M.H. Manghnani, J. Appl. Phys. **49**, 208 (1978).
[12] Y. Vohra and A. Ruoff, Phys. Rev. B **42**, 8651 (1990).
[13] A. Dewaele, M. Torrent, P. Loubeyre, and M. Mezouar, Phys. Rev. B **78**, 104102 (2008).
[14] K.D. Litasov, P.I. Dorogokupets, E. Ohtani, Y. Fei, A. Shatskiy, I.S. Sharygin, P.N. Gavryushkin, S.V. Rashchenko, Y.V. Seryotkin, Y. Higo, K. Funakoshi, A.D. Chanyshev, and S.S. Lobanov, J. Appl. Phys. **113**, 093507 (2013).
[15] Y. Akahama, N. Hirao, Y. Ohishi, and A.K. Singh, J. Appl. Phys. **116**, 223504 (2014).
[16] R.S. Hixson and J.N. Fritz, J. Appl. Phys. **71**, 1721 (1992).
[17] J.M. Walsh, M.H. Rice, R.G. McQueen, and F.L. Yarger, Phys. Rev. **108**, 196 (1957).
[18] R.G. McQueen, S.P. Marsh, J.W. Taylor, J.N. Fritz, and W.J. Carter, in *High Veloc. Impact Phenom.*, edited by R. Kinslow (Academic Press, New York, 1970), pp. 293–417.
[19] P.D. Asimow, D. Sun, and T.J. Ahrens, Phys. Earth Planet. Inter. **174**, 302 (2009).
[20] H. -k. Mao, P. Bell, J. Shaner, and D. Steinberg, J. Appl. Phys. **49**, 3276 (1978).
[21] S.M. Dorfman, V.B. Prakapenka, Y. Meng, and T.S. Duffy, J. Geophys. Res. **117**, B08210 (2012).
[22] M. Ross, D. Errandonea, and R. Boehler, Phys. Rev. B **76**, 184118 (2007).
[23] A. Belonoshko, S. Simak, A. Kochetov, B. Johansson, L. Burakovsky, and D. Preston, Phys. Rev. Lett. **92**, (2004).
[24] C. Cazorla, M.J. Gillan, S. Taioli, and D. Alfè, J. Chem. Phys. **126**, 194502 (2007).
[25] J.A. Moriarty, Phys. Rev. B **49**, 12431 (1994).
[26] M. Ross, L.H. Yang, and R. Boehler, Phys. Rev. B **70**, 184112 (2004).
[27] D. Errandonea, R. Boehler, and M. Ross, Phys. Rev. B **92**, 026101 (2015).
[28] T. Lukinov, S.I. Simak, and A.B. Belonoshko, Phys. Rev. B **92**, 060101 (2015).
[29] A. Salamat, R.A. Fischer, R. Briggs, M.I. McMahon, and S. Petitgirard, Coord. Chem. Rev. Press (2014).
[30] C.J. Wu, P. Soederlind, J.N. Glosli, and J.E. Klepeis, Nat. Mater. **8**, 223 (2009).
[31] D. Errandonea, M. Somayazulu, D. Häusermann, and H. -k. Mao, J. Phys. Condens. Matter **15**, 7635 (2003).
[32] S. Taioli, C. Cazorla, M. Gillan, and D. Alfè, Phys. Rev. B **75**, 214103 (2007).
[33] A.B. Belonoshko, R. Ahuja, and B. Johansson, Nature **424**, 1032 (2003).
[34] S. Anzellini, A. Dewaele, M. Mezouar, P. Loubeyre, and G. Morard, Science **340**, 464 (2013).
[35] R. Boehler, Nature **363**, 534 (1993).
[36] D. Alfè, M.J. Gillan, and G.D. Price, Nature **401**, 462 (1999).
[37] X. Zhang, Z. Liu, K. Jin, F. Xi, Y. Yu, Y. Tan, C. Dai, and L. Cai, J. Appl. Phys. **117**, 054302 (2015).
[38] L.B. Da Silva, P. Celliers, G.W. Collins, K.S. Budil, N.C. Holmes, T.W. Barbee Jr., B.A. Hammel, J.D. Kilkenny, R.J. Wallace, M. Ross, R. Cauble, A. Ng, and G. Chiu, Phys. Rev. Lett. **78**, 483 (1997).
[39] A. Benuzzi-Mounaix, M. Koenig, G. Huser, B. Faral, D. Batani, E. Henry, M. Tomasini, B. Marchet, T.A. Hall, M. Boustie, T.D. Rességuier, M. Hallouin, F. Guyot, D. Andrault, and T. Charpin, Phys. Plasmas 1994-Present **9**, 2466 (2002).
[40] D.K. Bradley, J.H. Eggert, R.F. Smith, S.T. Prisbrey, D.G. Hicks, D.G. Braun, J. Biener, A.V. Hamza, R.E. Rudd, and G.W. Collins, Phys. Rev. Lett. **102**, 075503 (2009).
[41] J. Hawreliak, H.E. Lorenzana, B.A. Remington, S. Lukezic, and J.S. Wark, Rev. Sci. Instrum. **78**, 083908 (2007).
[42] D. Milathianaki, J. Hawreliak, J.M. McNaney, B.S. El-Dasher, M.D. Saculla, D.C. Swift, H.E. Lorenzana, and T. Ditmire, Rev. Sci. Instrum. **80**, 093904 (2009).

[43] J.R. Rygg, J.H. Eggert, A.E. Lazicki, F. Coppari, J.A. Hawreliak, D.G. Hicks, R.F. Smith, C.M. Sorce, T.M. Uphaus, B. Yaakobi, and G.W. Collins, Rev. Sci. Instrum. **83**, 113904 (2012).
[44] A. Lazicki, J.R. Rygg, F. Coppari, R. Smith, D. Fratanduono, R.G. Kraus, G.W. Collins, R. Briggs, D.G. Braun, D.C. Swift, and J.H. Eggert, Phys. Rev. Lett. **115**, 075502 (2015).
[45] T.R. Boehly, D.L. Brown, R.S. Craxton, R.L. Keck, J.P. Knauer, J.H. Kelly, T.J. Kessler, S.A. Kumpan, S.J. Loucks, S.A. Letzring, F.J. Marshall, R.L. McCrory, S.F.B. Morse, W. Seka, J.M. Soures, and C.P. Verdon, Opt. Commun. **133**, 495 (1997).
[46] P.M. Celliers, D.K. Bradley, G.W. Collins, D.G. Hicks, T.R. Boehly, and W.J. Armstrong, Rev. Sci. Instrum. **75**, 4916 (2004).
[47] J.W. Forbes, *Shock Wave Compression of Condensed Matter* (Springer Berlin Heidelberg, Berlin, Heidelberg, 2012).
[48] K.K. Krupnikov, A.A. Bakanova, M.I. Brazhnik, and R.F. Trunin, Sov. Phys. Dokl. **8**, 205 (1963).
[49] R.G. McQueen and S.P. Marsh, J. Appl. Phys. **31**, 1253 (1960).
[50] S.P. Marsh, *LASL Shock Hugoniot Data* (University of California Press, 1980).
[51] L.V. Al'tshuler, M.N. Pavlovskii, L.V. Kuleshova, and G.V. Simakov, Fiz Tverd Tela 279 (1963).
[52] S.B. Kormer, M.V. Sinitsyn, A.I. Funtikov, V.D. Urlin, and A.V. Blinov, Zh Eksp Teor Fiz 1202 (1964).
[53] M. VAN Thiel, editor , *Compendium of Shock Wave Data.* (Lawrence Livermore Laboratory Report UCRL-50108, Livermore, 1977).
[54] F. Coppari, R.F. Smith, J.H. Eggert, J. Wang, J.R. Rygg, A. Lazicki, J.A. Hawreliak, G.W. Collins, and T.S. Duffy, Nat. Geosci. **6**, 926 (2013).
[55] J.R. Rygg, J.H. Eggert, A.E. Lazicki, F. Coppari, J.A. Hawreliak, D.G. Hicks, R.F. Smith, C.M. Sorce, T.M. Uphaus, B. Yaakobi, and G.W. Collins, Rev. Sci. Instrum. **83**, 113904 (2012).
[56] J.T. Larsen and S.M. Lane, J. Quant. Spectrosc. Radiat. Transf. **51**, 179 (1994).
[57] N. Christensen, A. Ruoff, and C. Rodriguez, Phys. Rev. B **52**, 9121 (1995).
[58] C. Dai, H. Tan, and H. Geng, J. Appl. Phys. **92**, 5019 (2002).
[59] X. Zhang, Z. Liu, Y. Gu, L. Cai, and F. Jing, Phys. B Condens. Matter **403**, 3261 (2008).
[60] S.-N. Luo and T.J. Ahrens, Phys. Earth Planet. Inter. **143–144**, 369 (2004).
[61] J.H. Nguyen, M.C. Akin, R. Chau, D.E. Fratanduono, W.P. Ambrose, O.V. Fat'yanov, P.D. Asimow, and N.C. Holmes, Phys. Rev. B **92**, 026102 (2015).
[62] D. Hayes, R. S. Hixon, and R. G. McQueen, in *Shock Compression of Condensed Matter*—1999, edited by M. D. Furnish, L. C. Chhabildas, and R. S. Hixon (American Institute of Physics, Melville, New York, 2000), p. 483.
[63] A. Dewaele, M. Mezouar, N. Guignot, and P. Loubeyre, Phys. Rev. Lett. **104**, 255701 (2010).
[64] B. Wang, G.B. Zhang, and Y.X. Wang, J. Alloys Compd. **556**, 116 (2013).
[65] J.E. Garcés, G.B. Grad, A. Fernández Guillermet, and S.J. Sferco, J. Alloys Compd. **289**, 1 (1999).

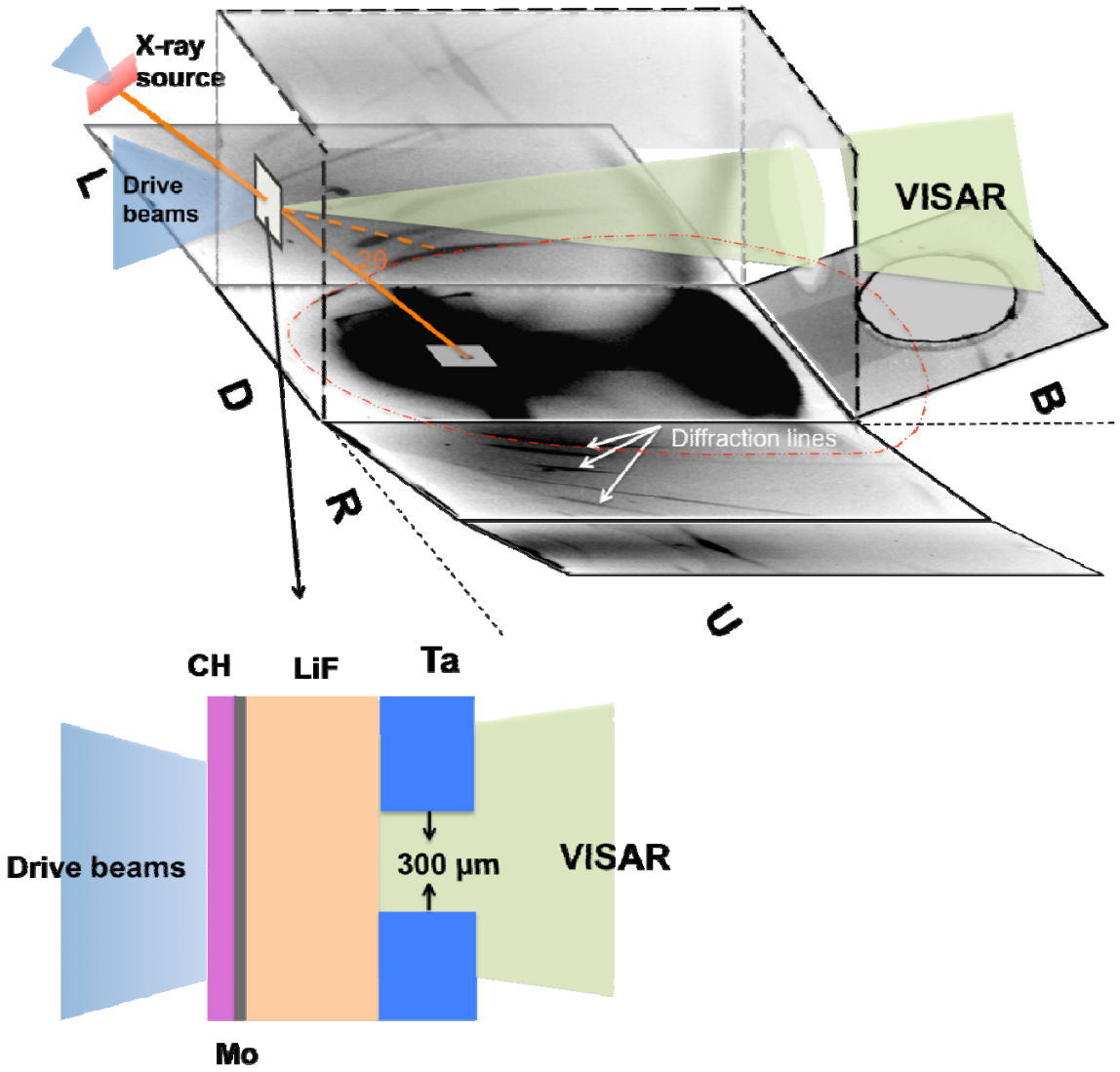

FIG.1 Experimental set-up for X-ray diffraction of shock-compressed molybdenum. The locations of the target package (white square), drive beams, X-ray source, and VISAR laser are indicated. The X-ray source is generated by laser ablation of a Cu foil shown in the upper left. A schematic of the target package is shown below. The X-ray diagnostic box lined with image plate detectors is shown here unfolded illustrating representative diffraction images. White arrows point to diffraction lines and the orange dash-dot line traces a representative diffraction peak across a series of image plates at a constant diffraction angle, 2θ. The panels are label L, R, U, D, B corresponding to the left, right, up, down, and back image plates.

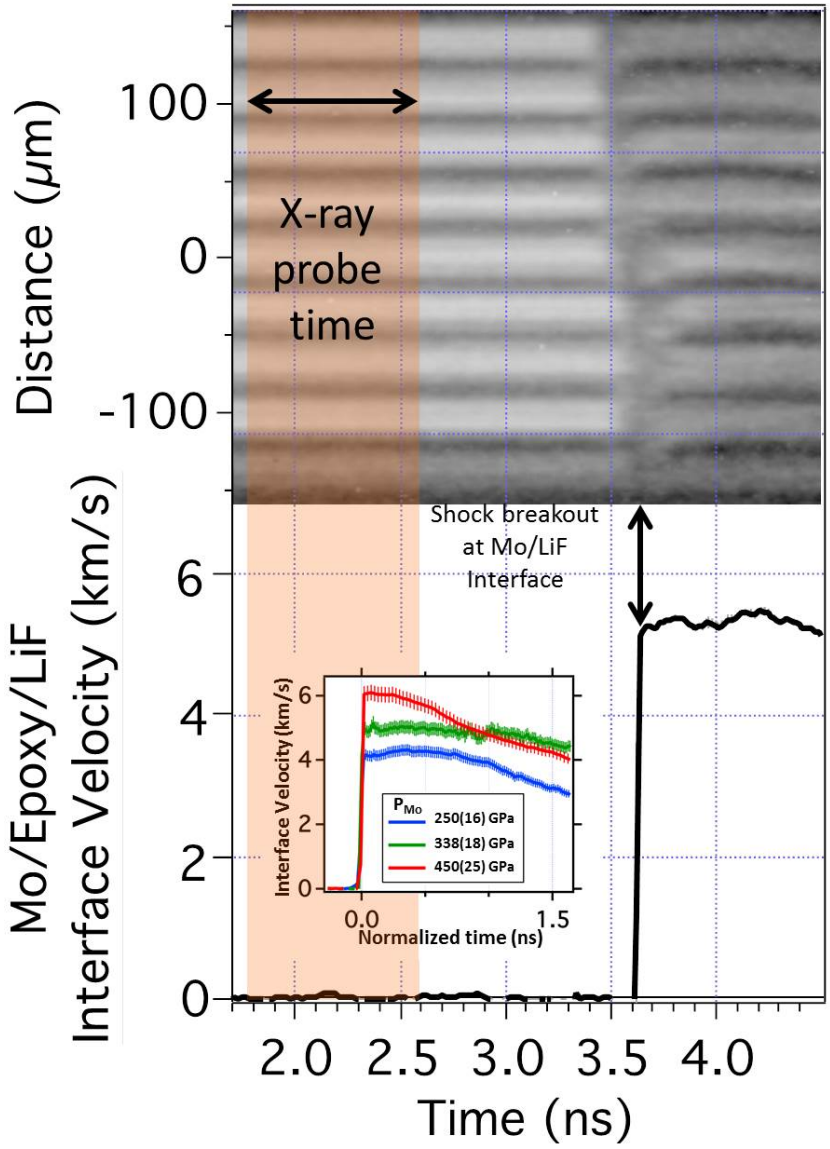

FIG.2 Representative VISAR interferogram recording the velocity at the interface between Mo and LiF for a calculated Mo pressure of 367(20) GPa (#s72418) (top panel). Blurring of the shock breakout is due wave reverberation into the epoxy layer used to glue the Mo foil to the LiF window. (Bottom panel) Extracted Mo/LiF velocity history from top panel. Small variations in interface velocity arise from fluctuations in the laser drive. The orange shaded area indicates the time the X-rays were generated relative to the wave propagation into the target package. Diffraction was measured before the wave breaks out into the LiF window and thus only part of the Mo sample is compressed. Inset shows additional representative extracted Mo/LiF velocities history from VISAR interferogram for calculated Mo pressures of 250(16) GPa (blue), 338 (18) GPa (green) and 450 (25) GPa (red). Time axis for each shot is normalized to shock arrival at Mo/LiF interface.

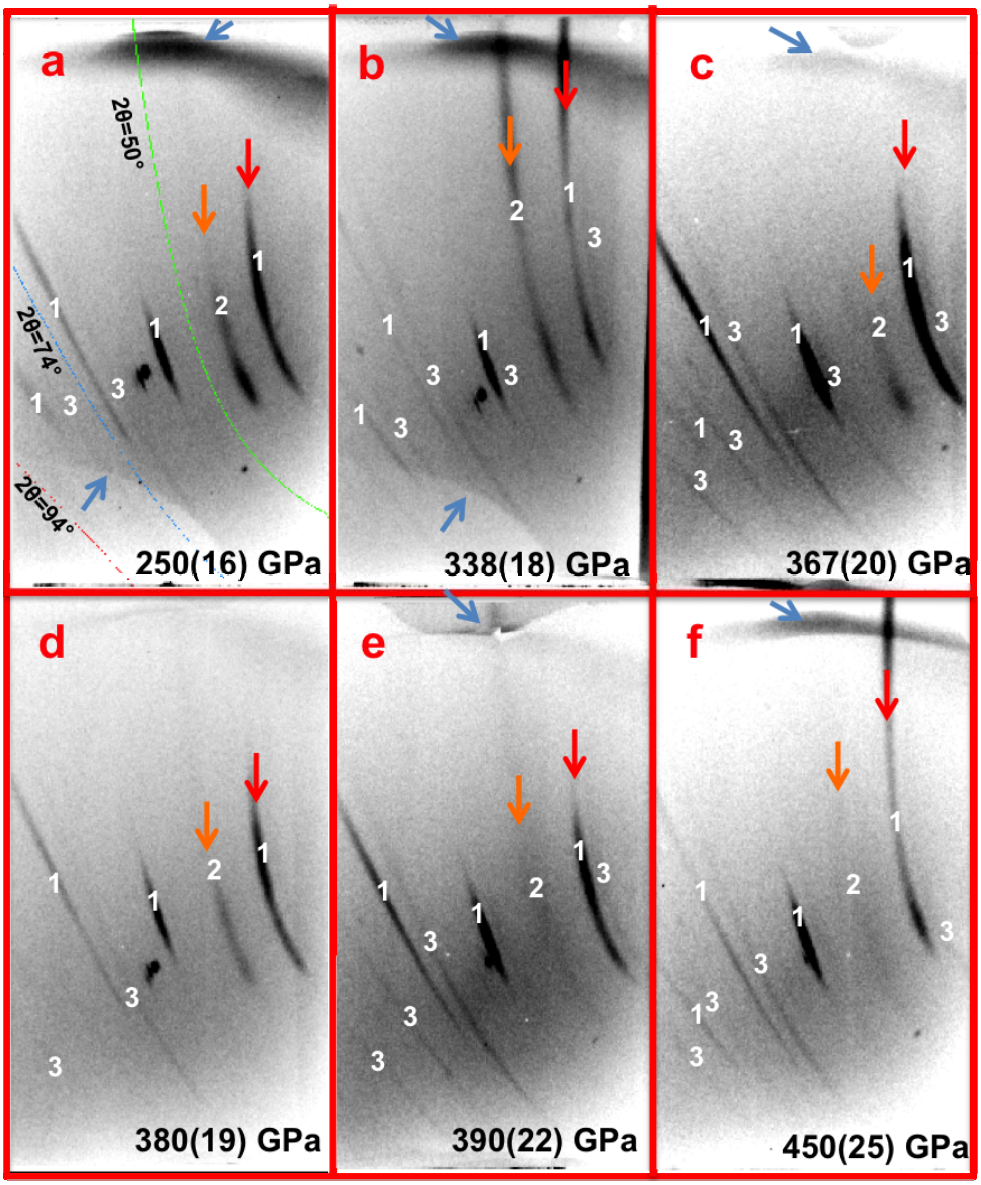

FIG.3 (a-f). Representative x-ray diffraction images from six Mo shock-compression experiments (left panel of Fig. 1). No background subtraction has been performed. The feature at the top and lower left indicated by blue arrows are artifacts from the filters inside the enclosure. The numbers indicate the assignments of the diffraction lines. 1: unshocked molybdenum 2: shocked molybdenum (orange arrow) 3: unshocked Ta. Single-crystal x-ray diffraction spots are suspected to arise from the LiF window. The green, blue and red curves in (a) show representative contours of constant 2θ at 50°, 74° and 94°.

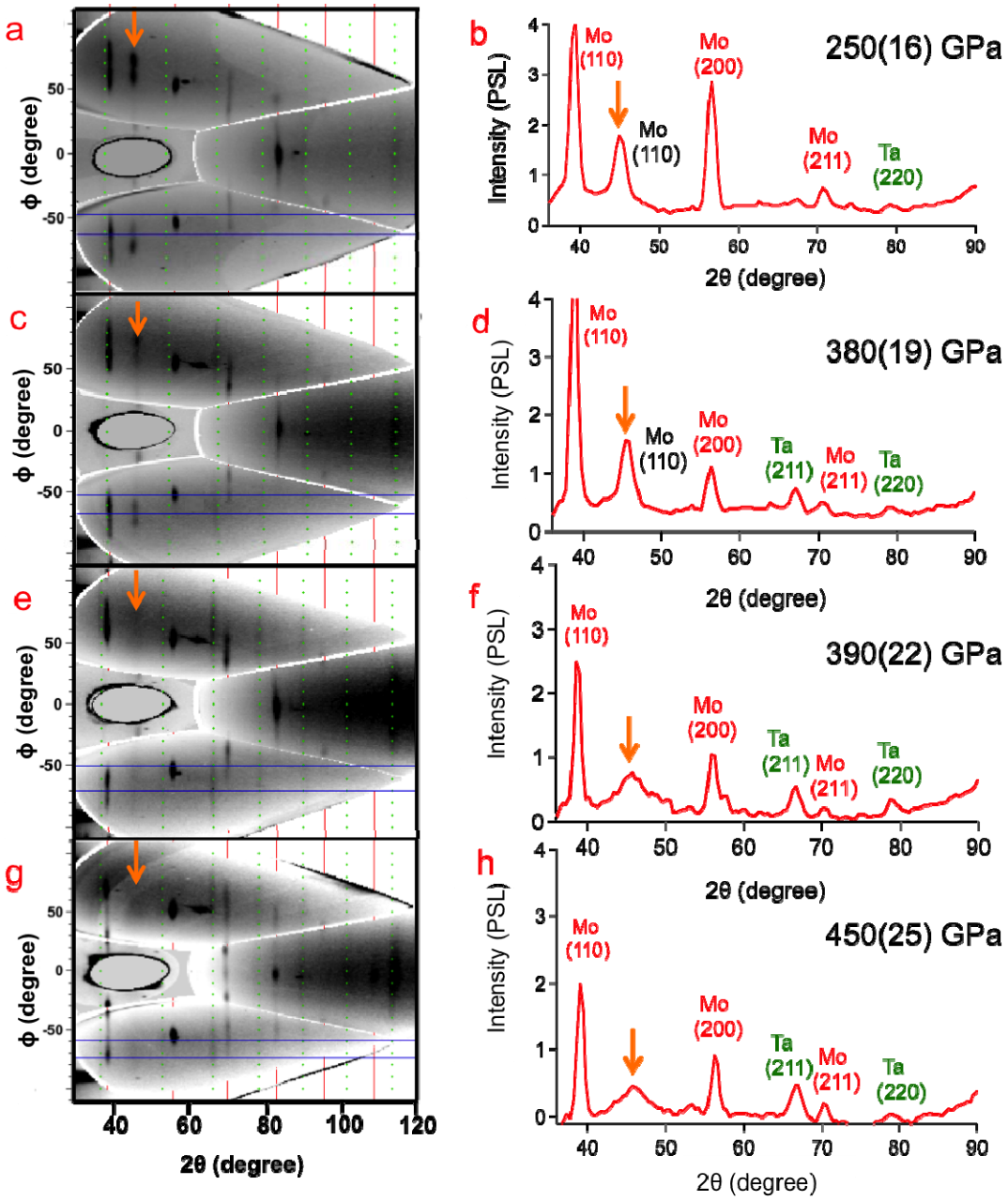

FIG.4 Representative X-ray diffraction data for shock-compressed Mo projected into 2θ-space[43], where is the azimuthal angle around the incident X-ray direction (panels a, c, e, and g). In these coordinates diffraction peaks are straight lines of constant 2θ. The vertical solid red lines and dashed green lines show positions of ambient-pressure Mo and Ta peaks, respectively. The orange arrows point to the location of the compressed Mo (110) peak for pressures below 380 GPa and diffuse scattering at higher pressures. The panels on the right (b, d, f and h) show the corresponding background-subtracted 1D X-ray diffraction patterns for the window regions defined by the horizontal blue lines on the corresponding left-hand panel. The diffraction peaks are assigned to uncompressed Mo (red labels), compressed Mo (black labels) and Ta pinhole (green labels). Intensities on the right hand panels are in photo-stimulated luminescence (PSL) units.

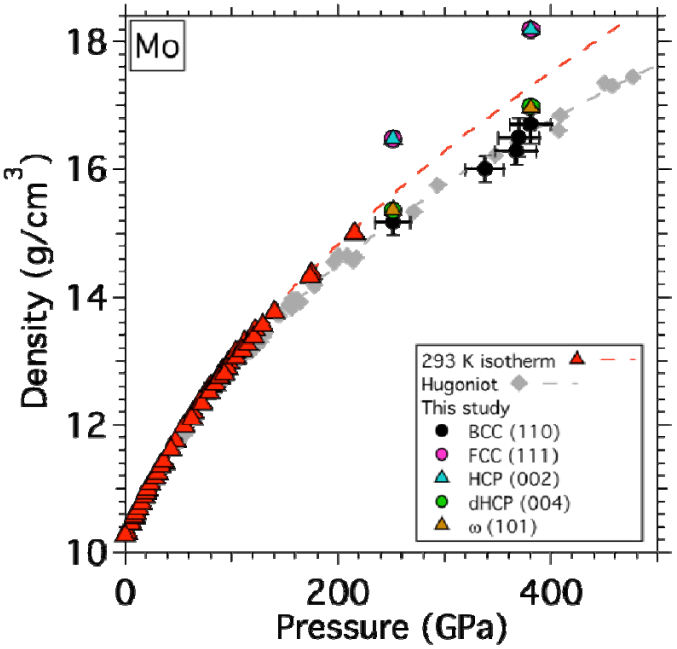

FIG.5 Pressure vs. density for molybdenum. Black circle shows results of X-ray densities from this study. Static diamond anvil cell data[13,21] are shown as red triangles and Hugoniot measurements[16–18,48,50] from gun experiments as grey diamonds. Densities are also shown for the FCC, HCP, dHCP, and ω phase at selected pressures by assigning the indicated diffraction line to the observed Mo diffraction peak. For hexagonal phases (HCP, dHCP, and ω), the c/a ratios are taken to be 1.633, 3.154 and 0.622, respectively[64,65]. Uncertainties are shown for BCC only and are similar for other structures.

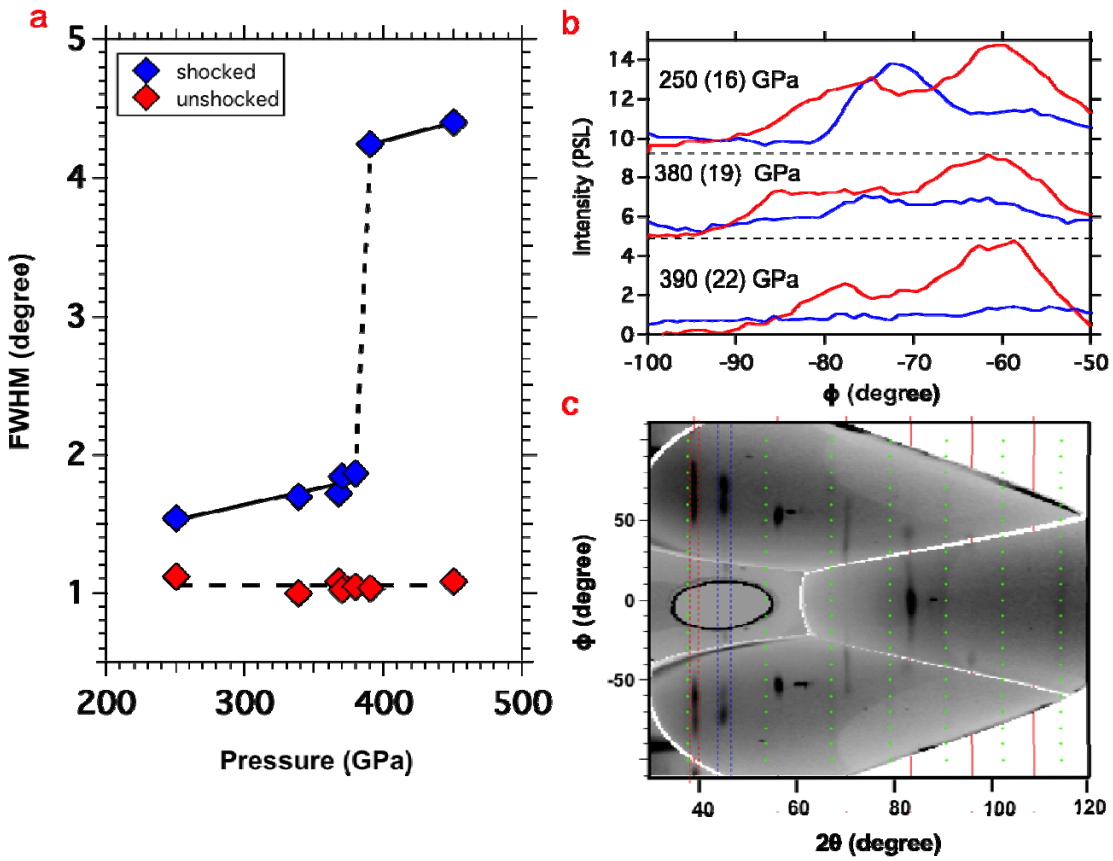

FIG.6 (a) Full width at half maximum (FWHM) of diffraction peaks vs. pressure for shocked and unshocked Mo. The blue diamonds show values from the diffraction feature near $2\theta \approx 45^{o}$ (the (110) peak up to 380 GPa and the diffuse scattering at high pressures). The FWHM of the shocked Mo (110) peak weakly increases from 1.6 to 1.9 ^{o} from 250-380 GPa and exhibits a sudden jump to values greater than 4^{o} above 390 GPa. The red diamonds show the FWHM of the corresponding unshocked Mo (110) peaks. (b) Intensity variations along the azimuthal direction ( ) relative to the incident X-ray beam for selected pressures. The red curves show the intensity variations of the (110) peak for the uncompressed regions of the Mo sample reflecting the texture of the starting foils. Azimuthal intensity variations of the compressed samples are shown as blue curves. At 250 GPa, the (110) peak of the compressed sample exhibits textural changes relative to the uncompressed sample. At 380 GPa, the compressed sample retains a reduced texture but no texturing can be observed at 390 GPa and above. Traces are offset for clarity with zero intensity values indicated by dashed black lines for offset traces. (c) Representative diffraction image (250 GPa) showing region of line-out (vertical red and blue dashed lines) between two-theta values of 38-40° and 45-47° used in panel (b). Background correction was performed by subtracting the intensity from an equal-sized line-out from immediately above or below the measured feature. The vertical solid red lines and dashed green lines show positions of ambient-pressure Mo and Ta peaks, respectively.

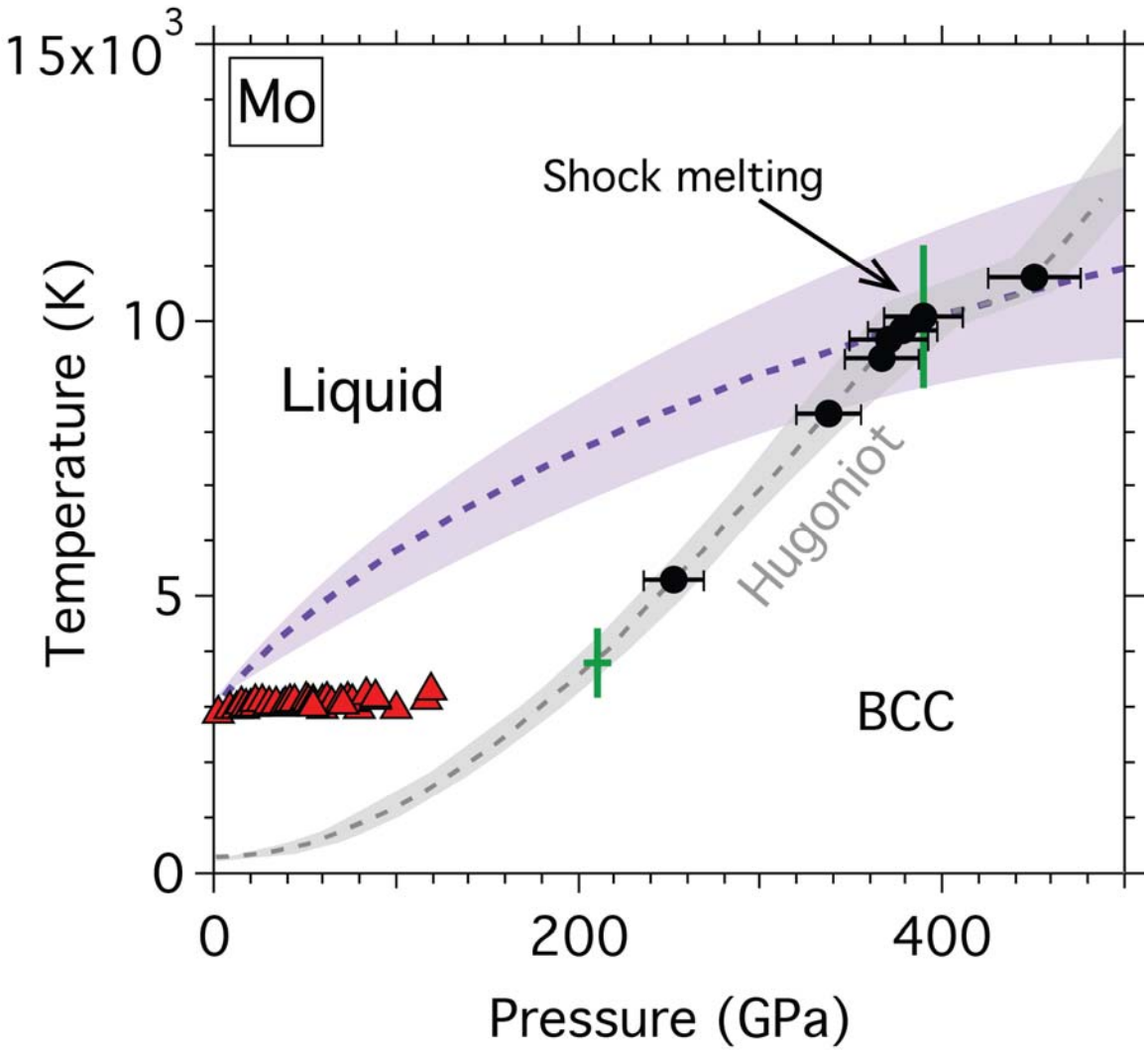

FIG.7 Phase diagram of molybdenum. Black circles represent our experimentally measured shock pressures and calculated shock temperatures[58] and the grey band shows the estimated uncertainty. The purple shaded region shows the range of calculated melting curves for Mo[4,8,24,58]. Red triangles show DAC melting data[1,3] and green bars indicate the location of previously reported 210-GPa and 390-GPa discontinuities with their uncertainties[2]. Black arrow points to where shock-melting is observed from our diffraction data at 390 GPa. The solid-liquid coexistence region is estimated from Ref. 58.

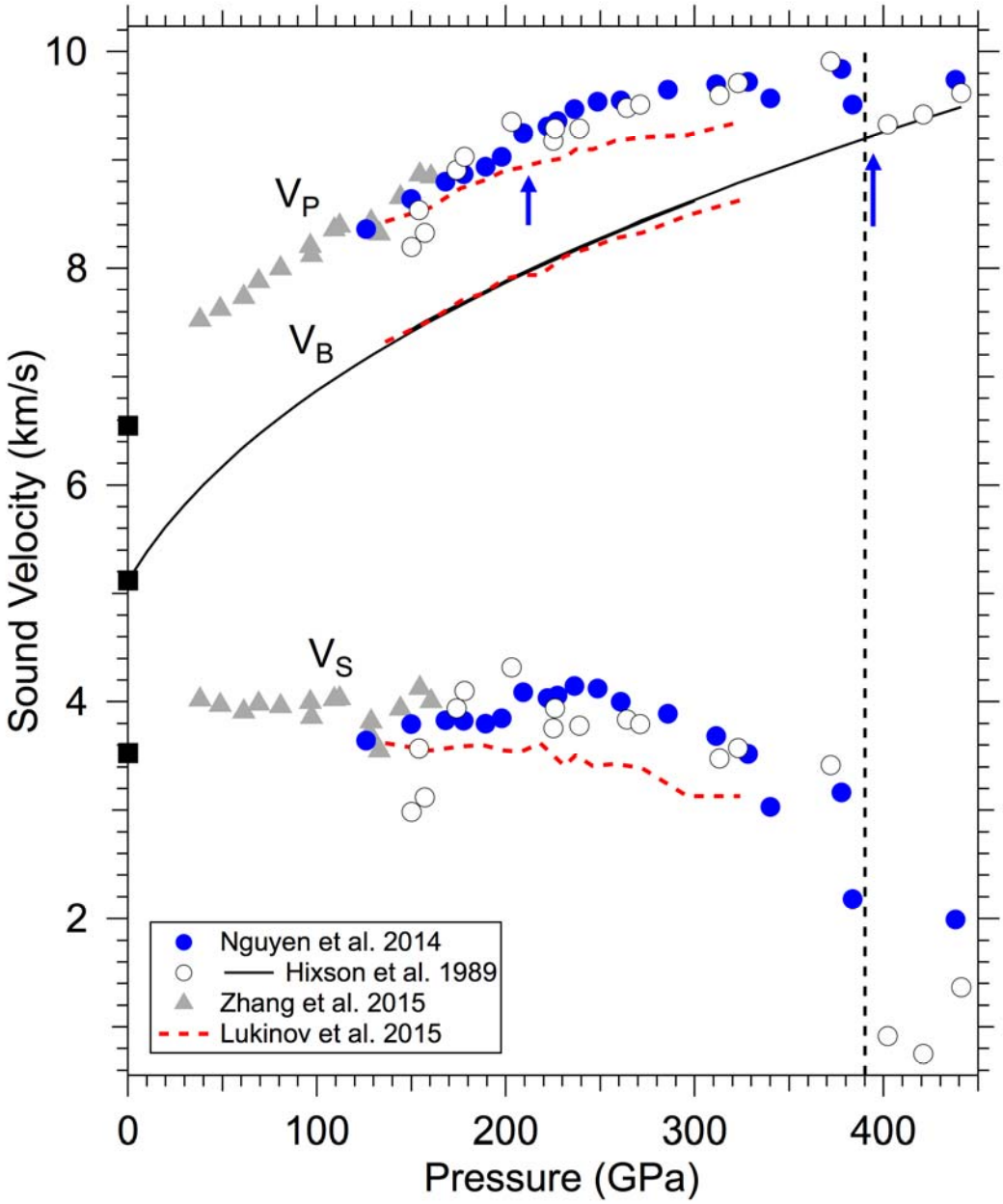

FIG. 8. Compressional (V_P), bulk (V_B), and shear (V_S) sound velocities in shocked molybdenum as a function of pressure. Blue, open and grey symbols are data obtained under shock compression from gas gun measurements using the optical analyzer technique[2,9,37]. Red dashed lines are from *ab initio* molecular dynamics calculations[28]. Black squares show 1-bar velocities. The solid black line shows bulk sound velocities calculated from the Hugoniot slope[2]. Blue arrows point to location of reported discontinuities at 210-GPa and 390-GPa[2]. More recent sound velocity data[9] provide additional evidence in support of the 390-GPa discontinuity consistent with our x-ray diffraction results (black dashed line) but do not support the existence of the 210-GPa discontinuity.

Table I. Hugoniot equation of state parameters used for impedance matching.

	Mo[16–18,48–50]	LiF[50–53]
ρ_0 (g/cm^3)	10.206	2.650
c (km/s)	5.11(2)	5.19(2)
s	1.247(5)	1.328(9)
γ_0	1.7	-

Table II. Results of X-ray diffraction experiments.

Shot #	u_{p_int} (km/s)	u_{p_Mo} (km/s)	Pressure (GPa)	d_{110} (Å)	X-ray Density (g/cm^3)
69814	4.09(16)	2.83(13)	250(16)	1.948(9)	15.2(2)
69816	4.99(18)	3.49(13)	338(18)	1.917(8)	16.0(2)
72418	5.26(19)	3.68(14)	367(20)	1.906(10)	16.3(2)
71106	5.28(19)	3.70(14)	370(20)	1.897(11)	16.5(3)
71114	5.38(19)	3.78(13)	380(19)	1.890(11)	16.7(3)
72416	5.47(19)	3.85(15)	390(22)	-	-
71112	5.99(20)	4.23(16)	450(25)	-	-

u_{p_int} - measured particle velocity at Mo/LiF interface, u_{p_Mo} - particle velocity in Mo from impedance match;d_{110} – d-spacing for (110) reflection of BCC Mo.